

1 Recurrent emergence and transmission of a SARS-CoV-2 Spike deletion Δ H69/V70

2

3 Kemp SA^{1,2,3}, Harvey WT⁴, Datir RP², Collier DA^{1,2,3}, Ferreira IATM^{2,3}, Carabelli AM³,
4 Robertson DL^{4,5}, Gupta RK^{2,3}

5

6 ¹Division of Infection and Immunity, University College London, London, UK.

7 ²Cambridge Institute of Therapeutic Immunology & Infectious Disease (CITIID), Cambridge,
8 UK.

9 ³Department of Medicine, University of Cambridge, Cambridge, UK.

10 ⁴MRC - University of Glasgow Centre for Virus Research, Glasgow, UK.

11 ⁵Institute of Biodiversity, Animal Health and Comparative Medicine, University of Glasgow,
12 Glasgow, UK

13

14

15 Address for correspondence:

16 Ravindra K. Gupta

17 Cambridge Institute for Therapeutic Immunology and Infectious Diseases

18 Jeffrey Cheah Biomedical Centre

19 Puddicombe Way

20 Cambridge CB2 0AW, UK

21 Tel: +44 1223 331491

22 rkg20@cam.ac.uk

23

24 Key words: SARS-CoV-2; COVID-19; antibody escape; neutralising antibodies; mutation;
25 evasion; resistance; fitness; evolution

26

27

28

29

30

31

32 **Abstract**

33 SARS-CoV-2 Spike amino acid replacements in the receptor binding domain (RBD) occur
34 relatively frequently and some have a consequence for immune recognition. Here we report
35 recurrent emergence and significant onward transmission of a six-nucleotide deletion in the
36 S gene, which results in loss of two amino acids: H69 and V70. Of particular note this
37 deletion, Δ H69/V70, often co-occurs with the receptor binding motif amino acid
38 replacements N501Y, N439K and Y453F. One of the Δ H69/V70+ N501Y lineages, B.1.1.7, is
39 comprised of over 1400 SARS-CoV-2 genome sequences from the UK and includes eight S
40 gene mutations: RBD (N501Y and A570D), S1 (Δ H69/V70 and Δ 144/145) and S2 (P681H,
41 T716I, S982A and D1118H). Some of these mutations have possibly arisen as a result of the
42 virus evolving from immune selection pressure in infected individuals and possibly only one
43 chronic infection in the case of lineage B.1.1.7. We find the Δ H69/V70 enhances viral
44 infectivity, indicating its effect on virus fitness is independent to the N501Y RBM change.
45 Enhanced surveillance for the Δ H69/V70 deletion with and without RBD mutations should
46 be considered as a priority. Such “permissive” mutations have the potential to enhance the
47 ability of SARS-CoV-2 to generate vaccine escape variants that would have otherwise
48 significantly reduced viral fitness.

49

50 **Background**

51 SARS-CoV-2's Spike surface glycoprotein engagement of hACE2 is essential for virus entry
52 and infection¹, and the receptor is found in respiratory and gastrointestinal tracts². Despite
53 this critical interaction and the constraints it imposes, it appears the RBD, and particularly
54 the receptor binding motif (RBM), can tolerate mutations^{3,4}, raising the real possibility of
55 virus escape from vaccine-induced immunity and monoclonal antibody treatments. Spike
56 mutants exhibiting reduced susceptibility to monoclonal antibodies have been identified in
57 *in vitro* screens^{5,6}, and some of these mutations have been found in clinical isolates⁷. Due to
58 the susceptibility of the human population to this virus, the acute nature of infections and
59 limited use of vaccines to date there has been limited selection pressure placed SARS-CoV-
60 2⁸; as a consequence few mutations that could alter antigenicity have increased significantly
61 in frequency.

62

63

64 The unprecedented scale of whole genome SARS-CoV-2 sequencing has enabled
65 identification and epidemiological analysis of transmission and surveillance, particularly in
66 the UK⁹. As of December 18th, there were 270,000 SARS-CoV-2 sequences available in the
67 GISAID Initiative (<https://gisaid.org/>). However, geographic coverage is very uneven with
68 some countries sequencing at higher rates than others. This could result in novel variants
69 with altered biological or antigenic properties evolving and not being detected until they are
70 already at high frequency.

71

72 Studying SARS-CoV-2 chronic infections can give insight into virus evolution that would
73 require many chains of acute transmission to generate. This is because the majority of
74 infections arise as a result of early transmission during pre or asymptomatic phases, and
75 virus adaptation not observed as it is naturally cleared by the immune response. We
76 recently documented *de novo* emergence of antibody escape mediated by S gene mutations
77 in an individual treated with convalescent plasma (CP)¹⁰. Dramatic changes in the
78 prevalence of Spike variants Δ H69/V70 (an out of frame six-nucleotide deletion) and D796H
79 variant followed repeated use of CP, while *in vitro* the mutated Δ H69/V70 variant displayed
80 reduced susceptibility to the CP and multiple other sera, at the same time retaining
81 infectivity comparable to wild type¹⁰. Worryingly, other deletions in the N-Terminal Domain
82 (NTD) have been reported to arise in chronic infections (ref Choi) and provide escape from
83 NTD-specific neutralising antibodies¹¹.

84

85 Here we analysed the available GISAID Initiative data for circulating SARS-CoV-2 Spike
86 sequences containing Δ H69/V70. We find, while occurring independently, the Spike
87 Δ H69/V70 often emerges after a significant RBM amino acid replacement that increases
88 binding affinity to hACE2. We present evidence that the Spike Δ H69/V70 is a fitness
89 enhancing change that may be stabilising other S gene mutations. Protein structure
90 modelling indicates this mutation could also contribute to antibody evasion as suggested for
91 other NTD deletions¹¹.

92

93 **Results**

94 The deletion H69/V70 is present in over 6000 sequences worldwide, 2.5% of the available
95 data (Figure 1), and largely in Europe from where most of the sequences in GISAID are

96 derived (Figure 2A). Many of the sequences are from the UK and Denmark where
97 sequencing rates are high compared to other countries. Δ H69/V70 occurs in variants
98 observed in different global lineages, representing multiple independent acquisitions of this
99 SARS-CoV-2 deletion (Figure 1). The earliest sample that includes the Δ H69/V70 was
100 detected in Sweden in April 2020 and is an independent deletion event relative to others.
101 The prevalence of Δ H69/V70 has since increased in other countries since August 2020
102 (Figure 2B, C). Further analysis of sequences revealed, firstly, that single deletions of either
103 69 or 70 were uncommon and secondly, some lineages of Δ H69/V70 alone were present
104 (Figure 1 and Figure 2A), as well as Δ H69/V70 in the context of other mutations in Spike,
105 specifically those in the RBM (Figure 2B and C).

106

107 To estimate the structural impact of Δ H69/V70, the structure of the NTD possessing the
108 double deletion was modelled. The Δ H69/V70 deletion was predicted to alter the
109 conformation of a protruding loop comprising residues 69 to 76, pulling it in towards the
110 NTD (Figure 3A). In the post-deletion structural model, the positions of the alpha carbons of
111 residues either side of the deleted residues, Ile68 and Ser71, were each predicted to occupy
112 positions 2.9Å from the positions of His69 and Val70 in the pre-deletion structure.
113 Concurrently, the positions of Ser71, Gly72, Thr73, Asn74 and Gly75 are predicted to have
114 changed by 6.5Å, 6.7Å, 6.0Å, 6.2Å and 8Å respectively, with the overall effect of drawing
115 these residues inwards, resulting in a less dramatically protruding loop. The position of this
116 loop in the pre-deletion structure is shown in the context of the wider NTD in Figure 3B. The
117 locations of main RBD mutations observed with Δ H69/V70 are shown in Figure 3C and D.
118 Residues belonging to a similarly exposed, nearby loop that form the epitope of a
119 neutralising, NTD-binding epitope are also highlighted.

120

121 We next examined the lineages where S gene mutations in the RBD were identified at high
122 frequency, in particular co-occurring with N439K, an amino acid replacement reported to be
123 defining variants increasing in numbers in Europe and detected across the world³ (Figure 4A,
124 Supplementary figure 1). N439K appears to have reduced susceptibility to a small subset of
125 monoclonals targeting the RBD, whilst retaining affinity for ACE2 *in vitro*³. The proportion of
126 viruses with Δ H69/V70 only increased from August 2020 when it appeared with the second
127 N439K lineage, B.1.141³ (Figure 4A). As of November 26th, remarkably there were twice as

128 many cumulative sequences with the deletion as compared to the single N439K indicating it
129 may be contributing to the success of this lineage (Figure 4A). Due to their high sampling
130 rates the country with the highest proportion of N439K+ Δ H69/V70 versus N439K alone is
131 England. The low levels of sequencing in most countries indicate N439K's prevalence could
132 be relatively high³. In Scotland, where early growth of N439K was high (forming N439K
133 lineage B.1.258 that subsequently went extinct with other lineages after the lockdown³),
134 there is now an inverse relationship with 546 versus 177 sequences for N439K and
135 N439K+ Δ H69/ Δ V70 respectively (as of November 26th). These differences therefore likely
136 reflect differing epidemic growth characteristics and timings of the introductions the N439K
137 variants with or without the deletion.

138

139 The second significant cluster with Δ H69/V70 and RBD mutants involves Y453F, another
140 RBD mutation that increases binding affinity to ACE2⁴ and has been found to be associated
141 with mink-human infections¹². In one SARS-CoV-2 mink-human sub-lineage, termed 'Cluster
142 5', Y453F and Δ H69/V70 occurred with F486L, N501T and M1229I and was shown to have
143 reduced susceptibility to sera from recovered COVID-19 patients (https://files.ssi.dk/Mink-cluster-5-short-report_AFO2). The Δ H69/V70 was first detected in the Y453F background on
144 August 24th and thus far appears limited to Danish sequences (supplementary figure 3).

146

147 A third lineage containing the same out of frame deletion Δ H69/V70 has arisen with
148 another RBD mutation N501Y (Figure 4B, Figure 5, supplementary figure 2). Based on its
149 location it might be expected to escape antibodies similar to COV2-2499⁵. In addition, when
150 SARS-CoV-2 was passaged in mice for adaptation purposes for testing vaccine efficacy,
151 N501Y emerged and increased pathogenicity¹³. Early sequences with N501Y alone were
152 isolated both in Brazil and USA in April 2020. N501Y + Δ H69/V70 sequences appear to have
153 been detected first in the UK in September 2020, with the crude cumulative number of
154 N501Y + Δ H69/V70 mutated sequences now exceeding the single mutant N501Y lineage
155 (Figure 4B). Of particular concern is a lineage (B.1.1.7) associated with relatively high
156 numbers of infections and currently around 1400 sequences (Figure 4C, Figure 5) with six S
157 mutations across the RBD (N501Y, A570D) and S2 (P681H, T716I, S982A and D1118H) as well
158 as the Δ H69/V70 and Δ 144 in England¹⁴ (Figure 6). This lineage has a very long branch
159 (Figure 5 and supplementary figure 3), suggestive of possible within host evolution.

160

161 The B.1.1.7 lineage (termed VUI 202012/01 by Public Health England) has some notable
162 features. Firstly the Δ 144 mutation that could lead to loss of binding of the S1 binding
163 antibody 4A8¹¹. Secondly the P681H mutation lies within the furin cleavage site. Furin
164 cleavage is a property of some more distantly related coronaviruses, and in particular not
165 found in SARS-CoV-1¹⁵. When SARS-CoV-2 is passaged *in vitro* it results in mutations in the
166 furin cleavage site, suggesting the cleavage is dispensable for *in vitro* infection¹⁶. The
167 significance of furin site mutations may be related to potential escape from the innate
168 immune antiviral IFITM proteins by allowing infection independent endosomes¹⁷. The
169 significance of the multiple S2 mutations is unclear at present, though D614G, also in S2 was
170 found to lead to a more open RBD orientation to explain its higher infectivity¹⁸. T716I and
171 D1118H occur at residues located close to the base of the ectodomain (Figure 6) that are
172 partially exposed and buried, respectively. The residue 982 is buried and located centrally,
173 in between the NTDs, at the top of a short helix (approximately residues 976-982) that is
174 completely shielded by the RBD when spike is in the closed form, though becomes slightly
175 more exposed in the open conformation. Residue 681 is part of a spike region that is
176 unmodelled in multiple published structures [Chi et al. 2020, Wrobel et al. 2020]. The
177 surface-exposed locations of modelled residues 676 and 689 (orange in Figure 6) suggest
178 the unmodelled residues 677-688 form a prominently-exposed loop that may be assumed to
179 show significant structural flexibility given the difficulties experienced in attaining an
180 accurate structural model of this region.

181

182 Given the association between Δ H69/V70 and other S gene mutations, we hypothesised
183 similar to our chronic infection¹⁰, that this deletion is enhancing virus infectivity. In the
184 absence of virus isolates we used a lentiviral pseudotyping approach to test the impact of
185 Δ H69/V70 on virus Spike protein mediated infection. A D614G bearing Spike protein
186 expressing DNA plasmid was co-transfected in HEK 293T producer cell lines along with
187 plasmids encoding lentiviral capsid and genome for luciferase. A mutant Spike bearing
188 Δ H69/V70 was also expressed in and infectious titres measured in supernatants from
189 producer cells (Figure 7). There was a significant difference in infectivity observed in the
190 Δ H69/V70 virus compared to wild type across multiple virus dilutions. When we adjusted
191 infectious titres to account for the amount of virus produced by wild type versus mutant in

192 the supernatants, a robust two fold increase of Δ H69/V70 over wild type was observed
193 (Figure 7).

194

195 **Discussion**

196 We have presented data demonstrating multiple, independent, and circulating lineages of
197 SARS-CoV-2 variants bearing a Spike Δ H69/V70. This deletion spanning six nucleotides, is
198 mostly due to an out of frame deletion of six nucleotides, has frequently followed receptor
199 binding amino acid replacements (N501Y, N439K and Y453F that have been shown to
200 increase binding affinity to hACE2 and reduce binding with monoclonal antibodies) and its
201 prevalence is rising in parts of Europe.

202

203 A recent analysis highlighted the potential for enhanced transmissibility of viruses with
204 deletions in the NTD, including Δ H69/V70¹¹. Here we show that the Δ H69/V70 deletion
205 increases Spike mediated infectivity by two-fold over a single round of infection. Over the
206 millions of replication rounds per day in a SARS-CoV-2 infection this is likely to be significant.
207 The potential for SARS-CoV-2 mutations to rapidly emerge and fix is exemplified by D614G,
208 an amino acid replacement in S2 that alters linkages between S1 and S2 subunits on
209 adjacent protomers as well as RBD orientation, infectivity, and transmission¹⁸⁻²⁰. The
210 example of D614G also demonstrates that mechanisms directly impacting important
211 biological processes can be indirect. Similarly, a number of possible mechanistic
212 explanations may underlie Δ H69/V70. For example, the fact that it sits on an exposed
213 surface and is estimated to alter the conformation of a particularly exposed loop might be
214 suggestive of immune interactions and escape, although allosteric interactions could
215 alternatively lead to higher infectivity.

216

217 The finding of a sub-lineage of over 1400 sequences bearing seven S gene mutations across
218 the RBD (N501Y, A570D), S1 (Δ H69/V70 and Δ 144) and S2 (P681H, T716I, S982A and
219 D1118H) in UK requires careful monitoring. The detection of a high number of novel
220 mutations suggests this lineage has either been introduced from a geographic region with
221 very poor sampling or viral evolution may have occurred in a single individual in the context
222 of a chronic infection¹⁰. This variant bears some concerning features; firstly the Δ H69/V70
223 deletion which we show to increase infectivity by two fold. Secondly the Δ 144 which may

224 affect binding by antibodies related to 4A8¹¹. Thirdly, the N501Y mutation that may have
225 higher binding affinity for ACE2 and a second RBD mutation A570D that could alter Spike
226 RBD structure. Finally, a mutation at the furin cleavage site could represent further
227 adaptative change.

228

229 Given the emergence of multiple clusters of variants carrying RBD mutations and the
230 Δ H69/V70 deletion, limitation of transmission takes on a renewed urgency. Continued
231 emphasis on testing/tracing, social distancing and mask wearing are essential, with
232 investment in other novel methods to limit transmission²¹. In concert, comprehensive
233 vaccination efforts in the UK and globally should be accelerated in order to further limit
234 transmission and acquisition of further mutations. If geographically limited then focussed
235 vaccination may be warranted. Research is vitally needed into whether lateral flow devices
236 for antigen and antibody detection can detect emerging strains and the immune responses
237 to them, particularly given reports that S signal in PCR based tests are frequently negative in
238 the new variant. Finally, detection of the deletion and other key mutations by rapid
239 diagnostics should be a research priority as such tests could be used as a proxy for antibody
240 escape mutations to inform surveillance at global scale.

241

242 **Acknowledgements**

243 RKG is supported by a Wellcome Trust Senior Fellowship in Clinical Science (WT108082AIA).
244 DLR is funded by the MRC (MC UU 1201412). WH is funded by the MRC (MR/R024758/1).
245 We thank Dr James Voss for the kind gift of HeLa cells stably expressing ACE2.

246

247 **Conflicts of interest**

248 RKG has received consulting fees from UMOVIS lab, Gilead Sciences and ViiV Healthcare,
249 and a research grant from InvisiSmart Technologies.

250

251 **Methods**

252 *Phylogenetic Analysis*

253 All available full-genome SARS-CoV-2 sequences were downloaded from the GISAID
254 database (<http://gisaid.org/>)²² on 26th November. Duplicate and low-quality sequences
255 (>5% N regions) were removed, leaving a dataset of 194,265 sequences with a length of

256 >29,000bp. All sequences were realigned to the SARS-CoV-2 reference strain MN908947.3,
257 using MAFFT v7.473 with automatic flavour selection and the --keeplength --addfragments
258 options²³. Major SARS-CoV-2 clade memberships were assigned to all sequences using the
259 Nextclade server v0.9 (<https://clades.nextstrain.org/>).

260

261 Maximum likelihood phylogenetic trees were produced using the above curated dataset
262 using IQ-TREE v2.1.2²⁴. Evolutionary model selection for trees were inferred using
263 ModelFinder²⁵ and trees were estimated using the GTR+F+I model with 1000 ultrafast
264 bootstrap replicates²⁶. All trees were visualised with Figtree v.1.4.4
265 (<http://tree.bio.ed.ac.uk/software/figtree/>), rooted on the SARS-CoV-2 reference sequence
266 and nodes arranged in descending order. Nodes with bootstraps values of <50 were
267 collapsed using an in-house script.

268

269 *Pseudotype virus preparation*

270 Viral vectors were prepared by transfection of 293T cells by using Fugene HD transfection
271 reagent (Promega). 293T cells were transfected with a mixture of 11ul of Fugene HD, 1µg of
272 pCDNAΔ19Spike-HA, 1ug of p8.91 HIV-1 gag-pol expression vector^{27,28}, and 1.5µg of pCSFLW
273 (expressing the firefly luciferase reporter gene with the HIV-1 packaging signal). Viral
274 supernatant was collected at 48 and 72h after transfection, filtered through 0.45um filter
275 and stored at -80°C as previously described²⁹. Infectivity was measured by luciferase
276 detection in target TZMBL transduced to express TMPRSS2 and ACE2.

277

278 *Normalisation of virus titre by SG-PERT to measure RT activity in lentivirus preparation*

279 Supernatant was subjected to SG-PERT as previously described³⁰.

280

281 *Structural modelling*

282 The structure of the post-deletion NTD (residues 14-306) was modelled using I-TASSER³¹, a
283 method involving detection of templates from the protein data bank, fragment structure
284 assembly using replica-exchange Monte Carlo simulation and atomic-level refinement of
285 structure using a fragment-guided molecular dynamics simulation. The structural model
286 generated was aligned with the spike structure possessing the pre-deletion conformation of

287 the 69-77 loop(PDB 7C2L³²) using PyMOL (Schrödinger). Figures prepared with PyMOL
288 using PDBs 7C2L, 6ZGE28 and 6ZGG³³.

289

290 **References**

- 291 1 Zhou, P. *et al.* A pneumonia outbreak associated with a new coronavirus of probable
292 bat origin. *nature* **579**, 270-273 (2020).
- 293 2 Sungnak, W. *et al.* SARS-CoV-2 entry factors are highly expressed in nasal epithelial
294 cells together with innate immune genes. *Nature medicine* **26**, 681-687 (2020).
- 295 3 Thomson, E. C. *et al.* The circulating SARS-CoV-2 spike variant N439K maintains
296 fitness while evading antibody-mediated immunity. *bioRxiv* (2020).
- 297 4 Starr, T. N. *et al.* Deep mutational scanning of SARS-CoV-2 receptor binding domain
298 reveals constraints on folding and ACE2 binding. *Cell* **182**, 1295-1310. e1220 (2020).
- 299 5 Greaney, A. J. *et al.* Complete mapping of mutations to the SARS-CoV-2 spike
300 receptor-binding domain that escape antibody recognition. *Cell Host & Microbe*
301 (2020).
- 302 6 Starr, T. N. *et al.* Prospective mapping of viral mutations that escape antibodies used
303 to treat COVID-19. *bioRxiv* (2020).
- 304 7 Choi, B. *et al.* Persistence and Evolution of SARS-CoV-2 in an Immunocompromised
305 Host. *New England Journal of Medicine* **383**, 2291-2293 (2020).
- 306 8 MacLean, O. A. *et al.* Natural selection in the evolution of SARS-CoV-2 in bats, not
307 humans, created a highly capable human pathogen. *BioRxiv* (2020).
- 308 9 consortiumcontact@cogconsortium.uk., C.-G. U. C.-U. An integrated national scale
309 SARS-CoV-2 genomic surveillance network. *Lancet Microbe* **1**, e99-e100,
310 doi:10.1016/s2666-5247(20)30054-9 (2020).
- 311 10 Kemp, S. *et al.* Neutralising antibodies drive Spike mediated SARS-CoV-2 evasion.
312 *medRxiv*, 2020.2012.2005.20241927, doi:10.1101/2020.12.05.20241927 (2020).
- 313 11 McCarthy, K. R. *et al.* Natural deletions in the SARS-CoV-2 spike glycoprotein drive
314 antibody escape. *bioRxiv*, 2020.2011.2019.389916, doi:10.1101/2020.11.19.389916
315 (2020).
- 316 12 Munnink, B. B. O. *et al.* Transmission of SARS-CoV-2 on mink farms between humans
317 and mink and back to humans. *Science* (2020).

- 318 13 Gu, H. *et al.* Adaptation of SARS-CoV-2 in BALB/c mice for testing vaccine efficacy.
319 *Science* **369**, 1603-1607, doi:10.1126/science.abc4730 (2020).
- 320 14 Rambaut A., L. N., Pybus O, Barclay W, Carabelli A. C., Connor T., Peacock T.,
321 Robertson D. L., Volz E., on behalf of COVID-19 Genomics Consortium UK (CoG-UK).
322 *Preliminary genomic characterisation of an emergent SARS-CoV-2 lineage in the UK*
323 *defined by a novel set of spike mutations*, <[https://virological.org/t/preliminary-](https://virological.org/t/preliminary-genomic-characterisation-of-an-emergent-sars-cov-2-lineage-in-the-uk-defined-by-a-novel-set-of-spike-mutations/563)
324 [genomic-characterisation-of-an-emergent-sars-cov-2-lineage-in-the-uk-defined-by-a-](https://virological.org/t/preliminary-genomic-characterisation-of-an-emergent-sars-cov-2-lineage-in-the-uk-defined-by-a-novel-set-of-spike-mutations/563)
325 [novel-set-of-spike-mutations/563](https://virological.org/t/preliminary-genomic-characterisation-of-an-emergent-sars-cov-2-lineage-in-the-uk-defined-by-a-novel-set-of-spike-mutations/563)> (2020).
- 326 15 Andersen, K. G., Rambaut, A., Lipkin, W. I., Holmes, E. C. & Garry, R. F. The proximal
327 origin of SARS-CoV-2. *Nature medicine* **26**, 450-452 (2020).
- 328 16 Davidson, A. D. *et al.* Characterisation of the transcriptome and proteome of SARS-
329 CoV-2 reveals a cell passage induced in-frame deletion of the furin-like cleavage site
330 from the spike glycoprotein. *Genome medicine* **12**, 1-15 (2020).
- 331 17 Peacock, T. P. *et al.* The furin cleavage site of SARS-CoV-2 spike protein is a key
332 determinant for transmission due to enhanced replication in airway cells. *bioRxiv*
333 (2020).
- 334 18 Yurkovetskiy, L. *et al.* Structural and functional analysis of the D614G SARS-CoV-2
335 spike protein variant. *Cell* **183**, 739-751. e738 (2020).
- 336 19 Korber, B. *et al.* Tracking changes in SARS-CoV-2 Spike: evidence that D614G
337 increases infectivity of the COVID-19 virus. *Cell* **182**, 812-827. e819 (2020).
- 338 20 Hou, Y. J. *et al.* SARS-CoV-2 D614G variant exhibits efficient replication ex vivo and
339 transmission in vivo. *Science* (2020).
- 340 21 Mlcochova, P. *et al.* Extended in vitro inactivation of SARS-CoV-2 by titanium dioxide
341 surface coating. *bioRxiv* (2020).
- 342 22 Shu, Y. & McCauley, J. GISAID: Global initiative on sharing all influenza data - from
343 vision to reality. *Euro surveillance : bulletin Europeen sur les maladies transmissibles*
344 *= European communicable disease bulletin* **22**, 30494, doi:10.2807/1560-
345 7917.ES.2017.22.13.30494 (2017).
- 346 23 Katoh, K. & Standley, D. M. MAFFT Multiple Sequence Alignment Software Version 7:
347 Improvements in Performance and Usability. *Molecular Biology and Evolution* **30**,
348 772-780, doi:10.1093/molbev/mst010 (2013).

- 349 24 Minh, B. Q. *et al.* IQ-TREE 2: New Models and Efficient Methods for Phylogenetic
350 Inference in the Genomic Era. *Molecular Biology and Evolution* **37**, 1530-1534,
351 doi:10.1093/molbev/msaa015 (2020).
- 352 25 Kalyaanamoorthy, S., Minh, B. Q., Wong, T. K., von Haeseler, A. & Jermini, L. S.
353 ModelFinder: fast model selection for accurate phylogenetic estimates. *Nature*
354 *methods* **14**, 587-589 (2017).
- 355 26 Minh, B. Q., Nguyen, M. A. T. & von Haeseler, A. Ultrafast Approximation for
356 Phylogenetic Bootstrap. *Molecular Biology and Evolution* **30**, 1188-1195,
357 doi:10.1093/molbev/mst024 (2013).
- 358 27 Naldini, L., Blömer, U., Gage, F. H., Trono, D. & Verma, I. M. Efficient transfer,
359 integration, and sustained long-term expression of the transgene in adult rat brains
360 injected with a lentiviral vector. *Proceedings of the National Academy of Sciences* **93**,
361 11382-11388 (1996).
- 362 28 Gupta, R. K. *et al.* Full length HIV-1 gag determines protease inhibitor susceptibility
363 within in vitro assays. *AIDS (London, England)* **24**, 1651 (2010).
- 364 29 Mlcochova, P. *et al.* Combined Point-of-Care Nucleic Acid and Antibody Testing for
365 SARS-CoV-2 following Emergence of D614G Spike Variant. *Cell Reports Medicine* **1**,
366 100099 (2020).
- 367 30 Gregson, J. *et al.* HIV-1 viral load is elevated in individuals with reverse transcriptase
368 mutation M184V/I during virological failure of first line antiretroviral therapy and is
369 associated with compensatory mutation L74I. *Journal of Infectious Diseases* (2019).
- 370 31 Roy, A., Kucukural, A. & Zhang, Y. I-TASSER: a unified platform for automated protein
371 structure and function prediction. *Nature protocols* **5**, 725-738 (2010).
- 372 32 Chi, X. *et al.* A neutralizing human antibody binds to the N-terminal domain of the
373 Spike protein of SARS-CoV-2. *Science* **369**, 650-655 (2020).
- 374 33 Wrobel, A. G. *et al.* SARS-CoV-2 and bat RaTG13 spike glycoprotein structures inform
375 on virus evolution and furin-cleavage effects. *Nature Structural & Molecular Biology*
376 **27**, 763-767, doi:10.1038/s41594-020-0468-7 (2020).
- 377

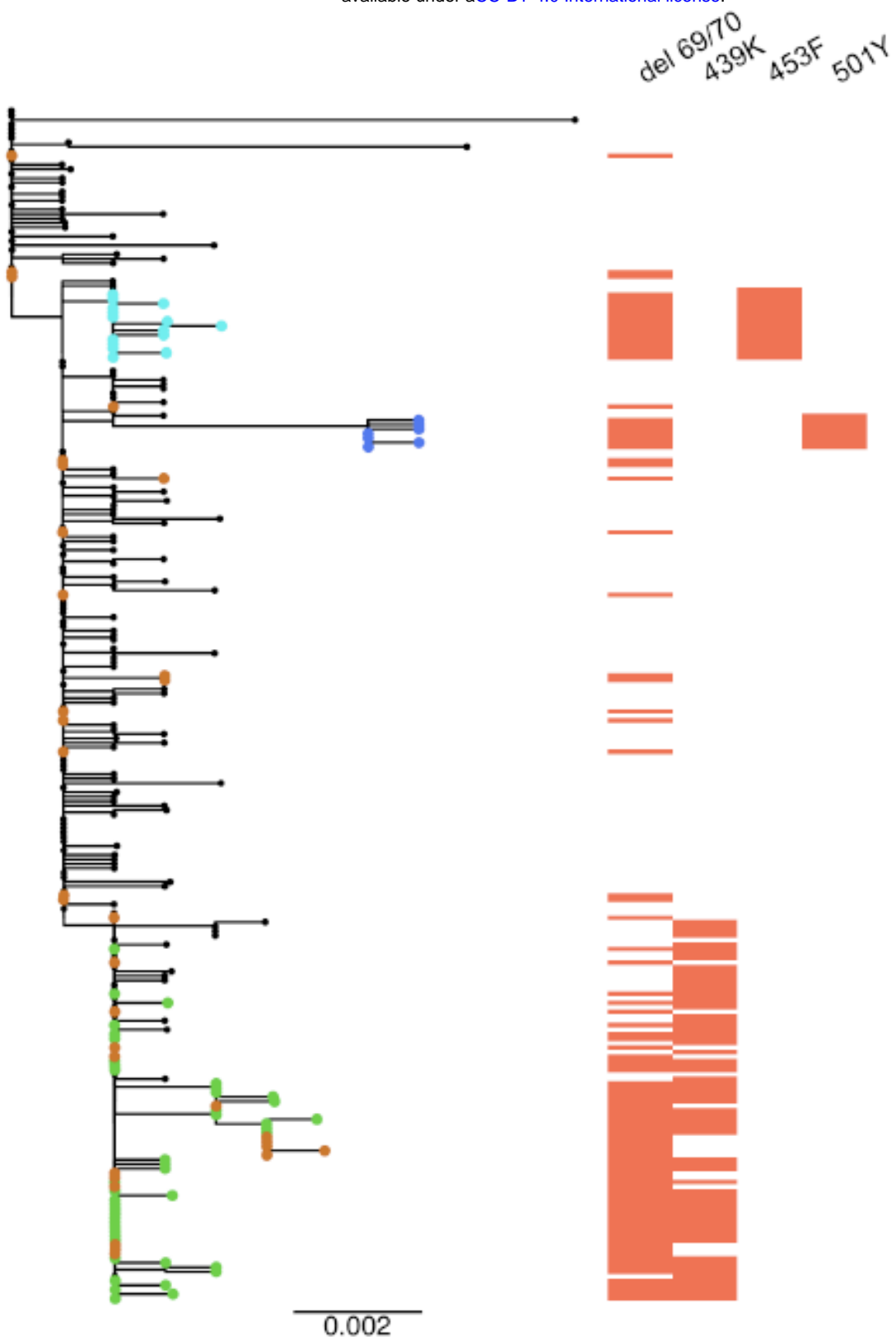
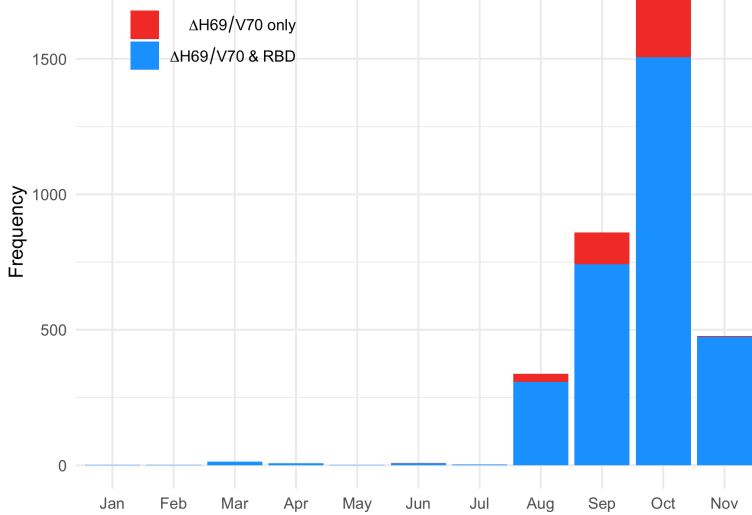
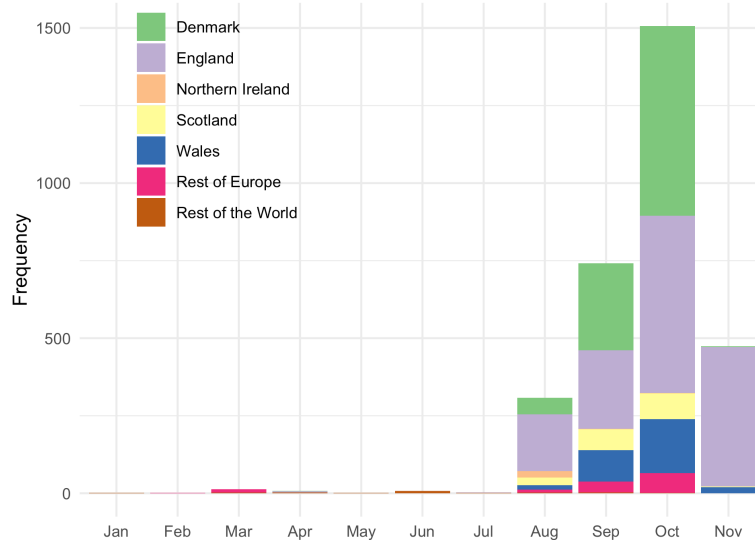


Figure 1. Global whole genome phylogeny of SARS-CoV-2 sequences highlighting those with specific mutations in Spike. All sequences containing four major spike mutations ($\Delta 69/70$, N439K, Y453F and 501Y) were downloaded from the GISAID database. Duplicate sequences were removed and subsampled. Tree tips are coloured as follows; brown, $\Delta 69/70$; cyan $\Delta 69/70 + Y453F$; blue, $\Delta 69/70 + N501Y$; green $\Delta 69/70 + 439K$; remainder in black. Columns showing presence or absence of deletion and amino acid variants N439K, Y453F, and N501Y matching the tip labelling.

A



B



C

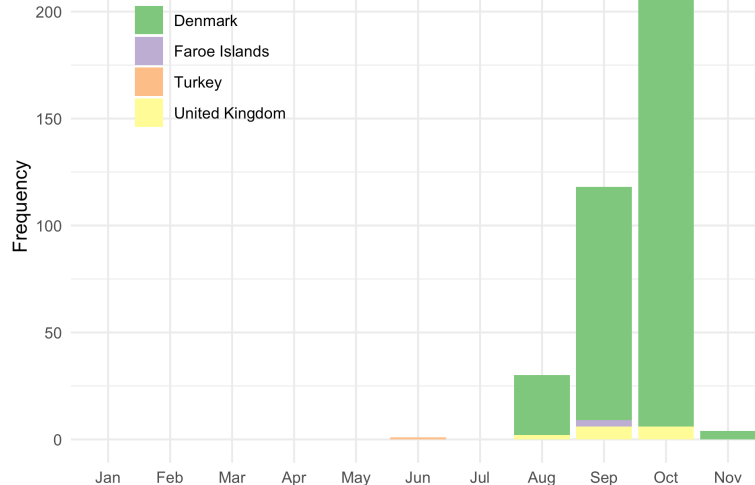
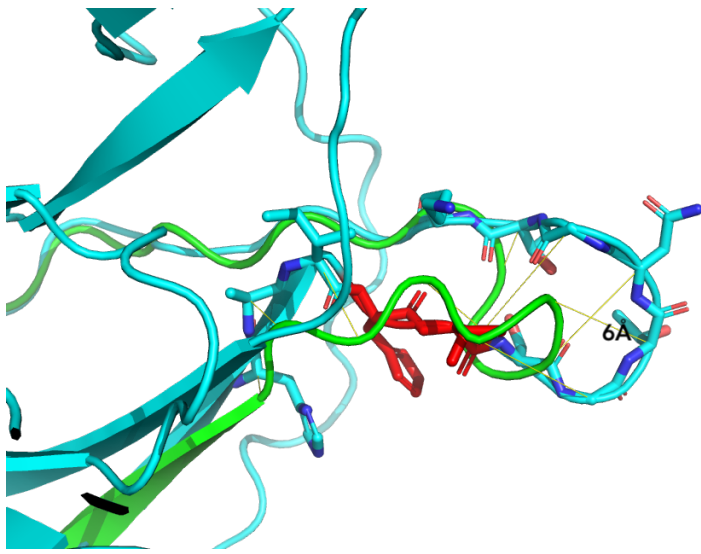
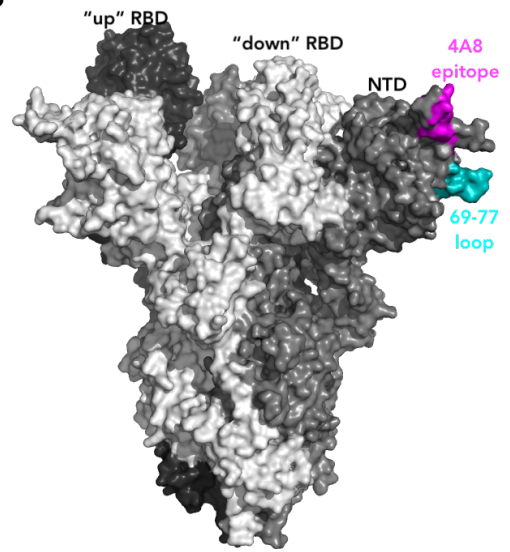


Figure 2. Number of new occurrences of SARS-CoV-2 sequences with the $\Delta H69/V70$ Δ etion. All sequences containing the $\Delta H69/V70$ Δ etion were extracted from the GISAID database (Accessed 16th Dec 2020) and tabulated according to both reporting country of origin and date in which they were deposited in the database. The frequency of viruses carrying the $\Delta H69/V70$ Δ etion rose substantially from August to present. **A.** Worldwide carriage of $\Delta H69/V70$; most sequences preferentially carry RBD mutations alongside the Δ etion. **B.** Several distinct $\Delta H69/V70$ lineages carrying RBD mutations 439K, 453F and 501Y have begun to emerge, predominantly in Denmark and England. **C.** Sequences carrying the $\Delta H69/V70$ but in the absence of other major Spike mutations are restricted mostly to Denmark.

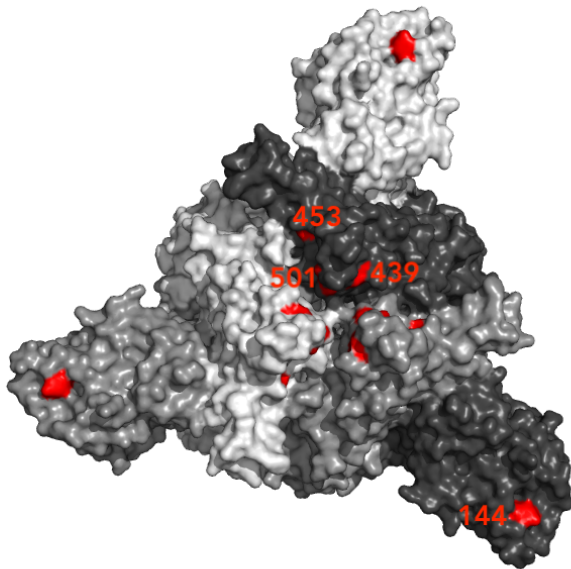
A



B



C



D

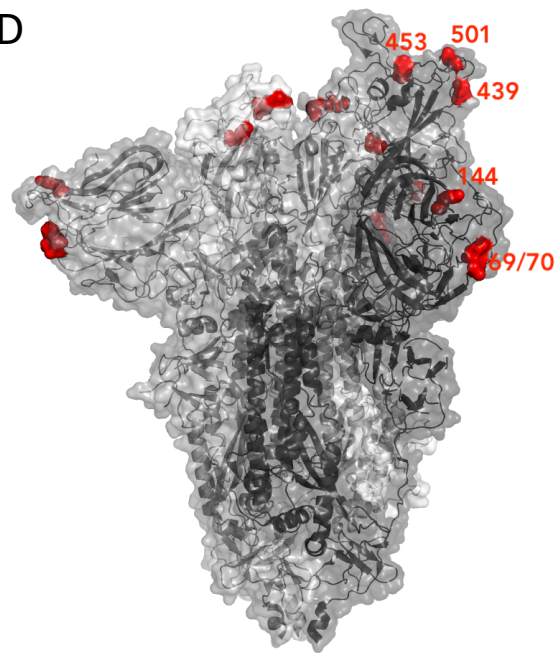


Figure 3. **A)** Prediction of conformational change in the spike N-terminal domain due to Δ etion of residues His69 and Val70. The pre- Δ etion structure is shown in cyan, except for residues 69 and 70, which are shown in red. The predicted post- Δ etion structure is shown in green. Residues 66-77 of the pre- Δ etion structure are shown in stick representation and coloured by atom (carbon in cyan, nitrogen in blue, oxygen in coral). Yellow lines connect aligned residues 66-77 of the pre- and post- Δ etion structures and the distance of 6 Å between aligned alpha carbons of Thr73 in the pre- and post- Δ etion conformation is labelled. **B)** Surface representation of spike homotrimer in open conformation (PDB: 7C2L) with each monomer shown in different shades of grey. On the monomer shown positioned to the right, the exposed loop consisting of residues 69-77 is shown in cyan and the neutralising antibody (4A8) binding NTD epitope described by Chi et al. is shown in magenta **C)** Surface representation of spike homotrimer in closed conformation (PDB: 6ZGE., 2020) homotrimer viewed in a 'top-down' view along the trimer axis. The locations of RBD mutations at residues 439, 453 and 501 and the Δ etion at Tyr144 are highlighted in red and labelled on a single monomer. **D)** Spike in open conformation with a single erect RBD (PDB: 6ZGG) in trimer axis vertical view with the locations of Δ eted residues His69 and Val70 in the N-terminal domain and RBD mutations highlighted as red spheres and labelled on the monomer with erect RBD. Residues 71-75, which form the exposed loop undergoing conformational change in **A**, are omitted from this structure.

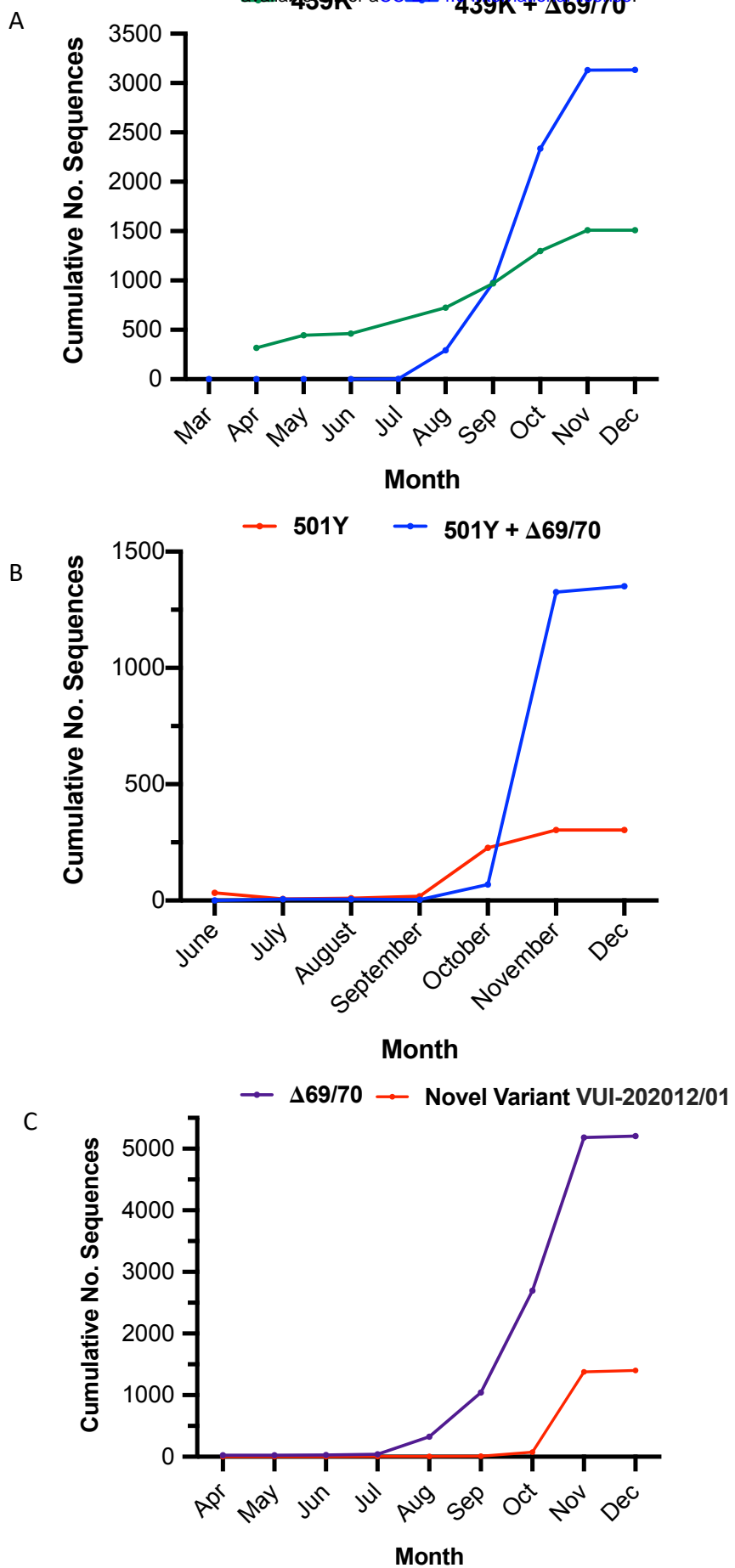


Figure 4. The relative increase in frequency of sequences carrying Spike mutants 439K (A), 501Y (B) and $\Delta 69/70$ (C) based on sampling dates. In lineages carrying 439K and 501Y, viruses co-carrying the $\Delta 69/70$ Δ etion became dominant between September-October 2020 in terms of cumulative cases. The novel variant, lineage B.1.1.7 carrying eight linked Spike mutations is increasing in frequency.

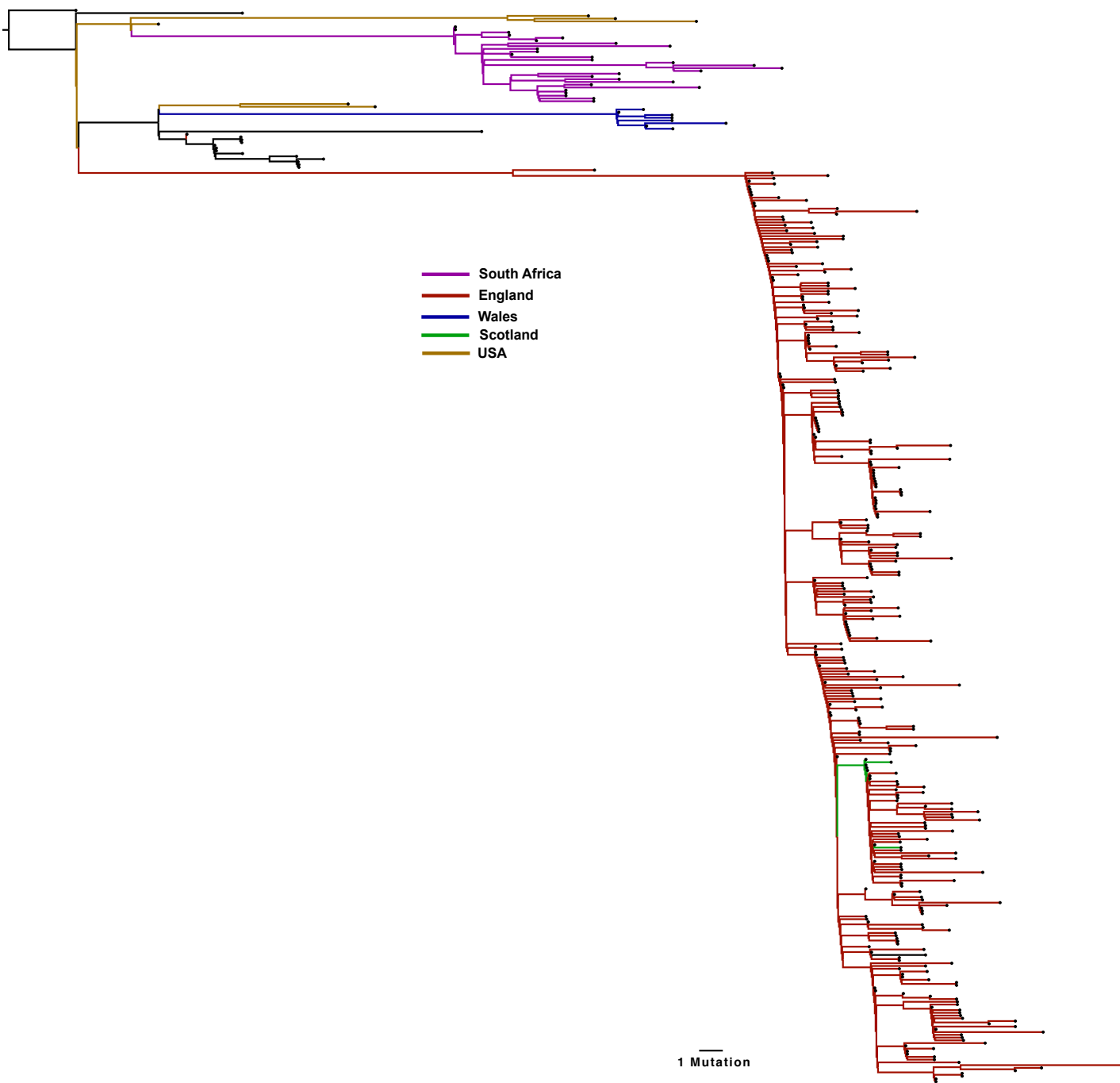


Figure 5. Divergence of global lineages bearing Spike 501Y mutation: A global maximum likelihood phylogeny of all SARS-CoV-2 sequences bearing the 501Y mutations were downloaded from the GISAID database (2000 sequences, accessed 16th December 2020). All duplicate sequences were removed to create a representative sub-sample of sequences. Distinct sub-lineages of the Spike 501Y variants are currently circulating in the UK (predominantly England, red), with significant expansion also occurring in South Africa (pink).

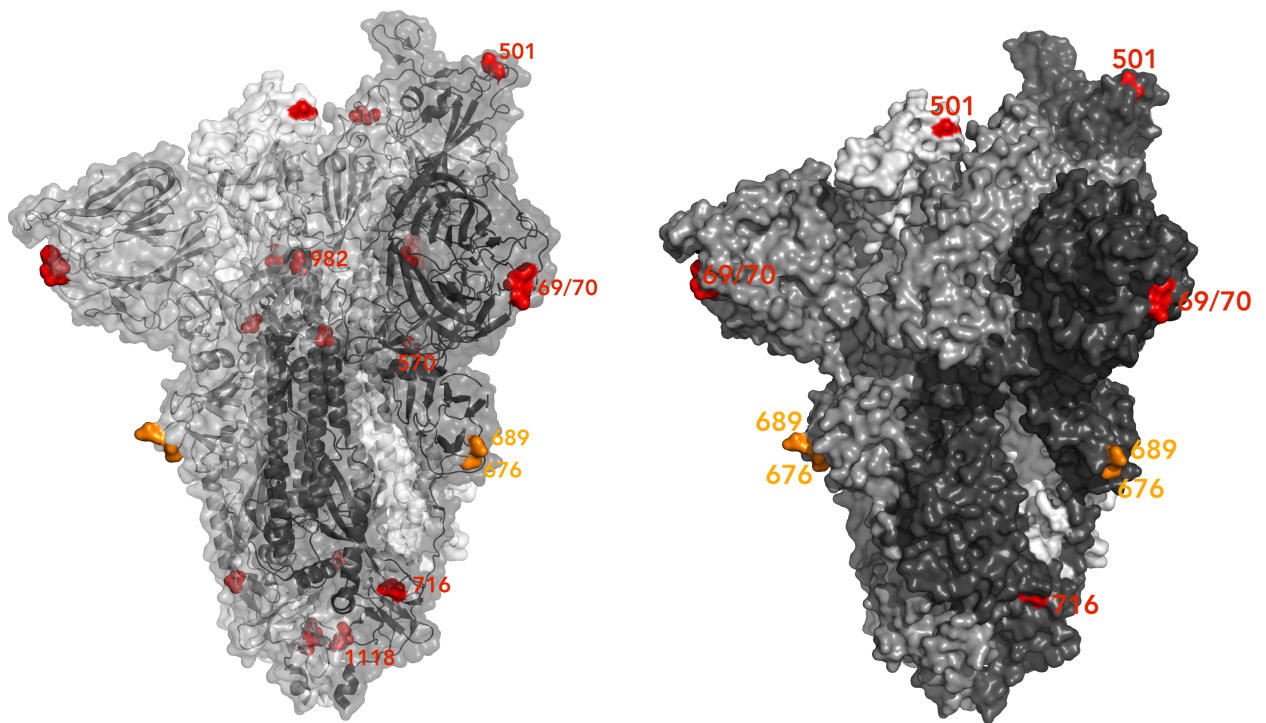


Figure 6. Spike residues in a highly mutated circulating virus VUI 202012/01 with Δ H69/V70. Spike homotrimer in open conformation with one upright RBD (PDB: 6ZGE, Wrobel et al., 2020) with different monomers shown in shades of grey. To the left, surface representation overlaid with ribbon representation and to the right, opaque surface representation accentuating the locations of surface-exposed residues. The Δ eted residues 69 and 70 and the residues involved in amino acid substitutions (501, 570, 716, 982 and 1118) are coloured red. The location of an exposed loop including residue 681 is absent from the structure, though the residues either side of the unmo Δ led residues, 676 and 689, are coloured orange. On the left structure, highlighted residues are labelled on the monomer with an upright RBD; on the right structure, all visible highlighted residues are labelled.

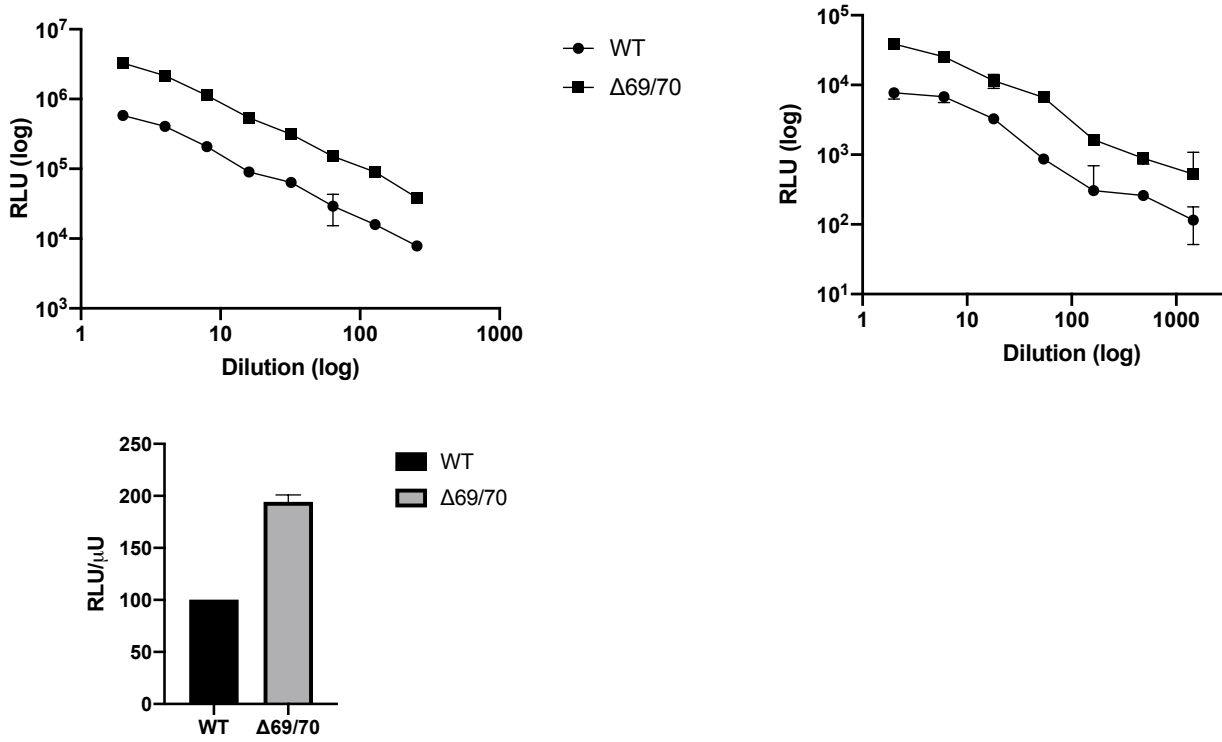
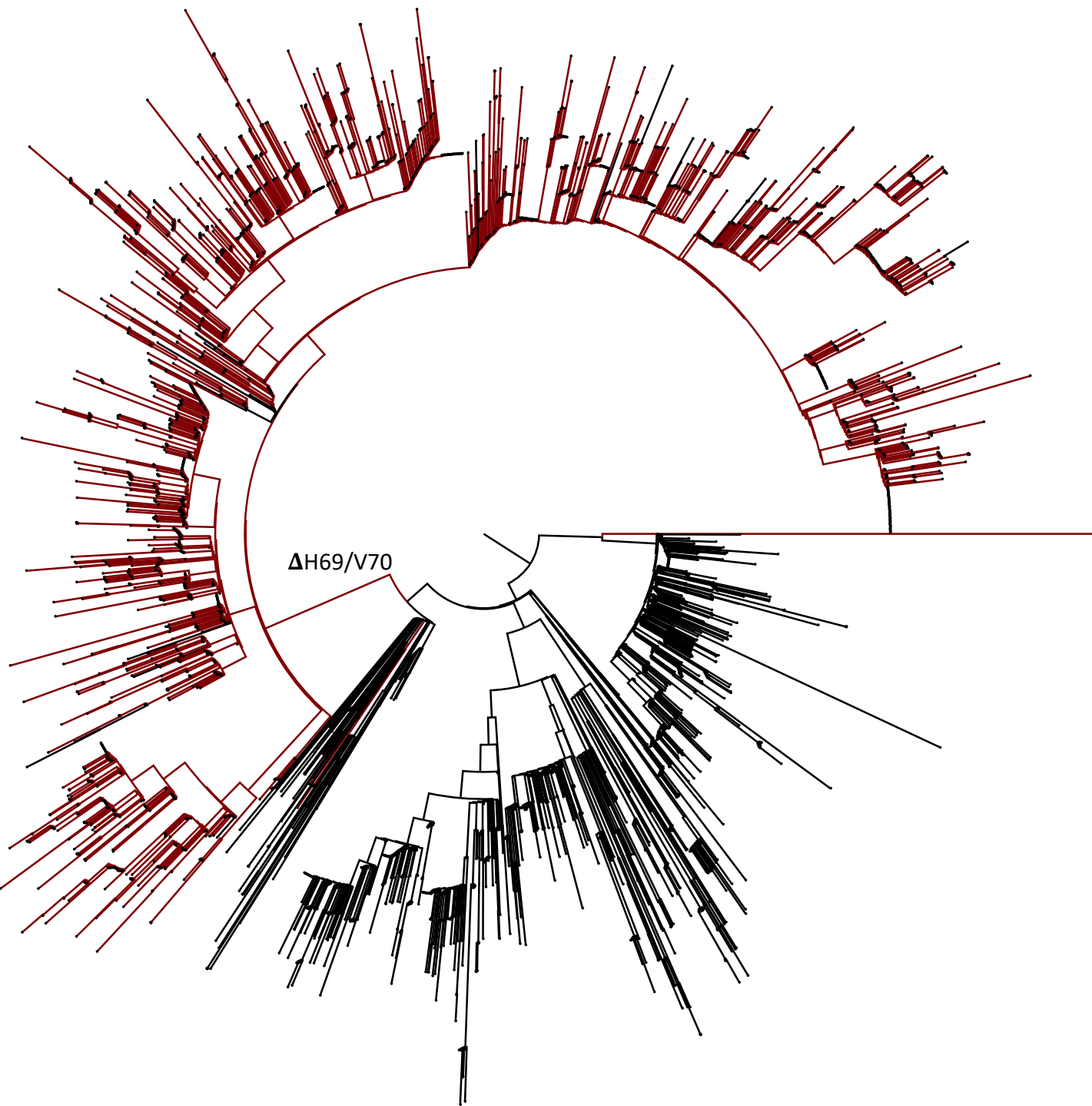
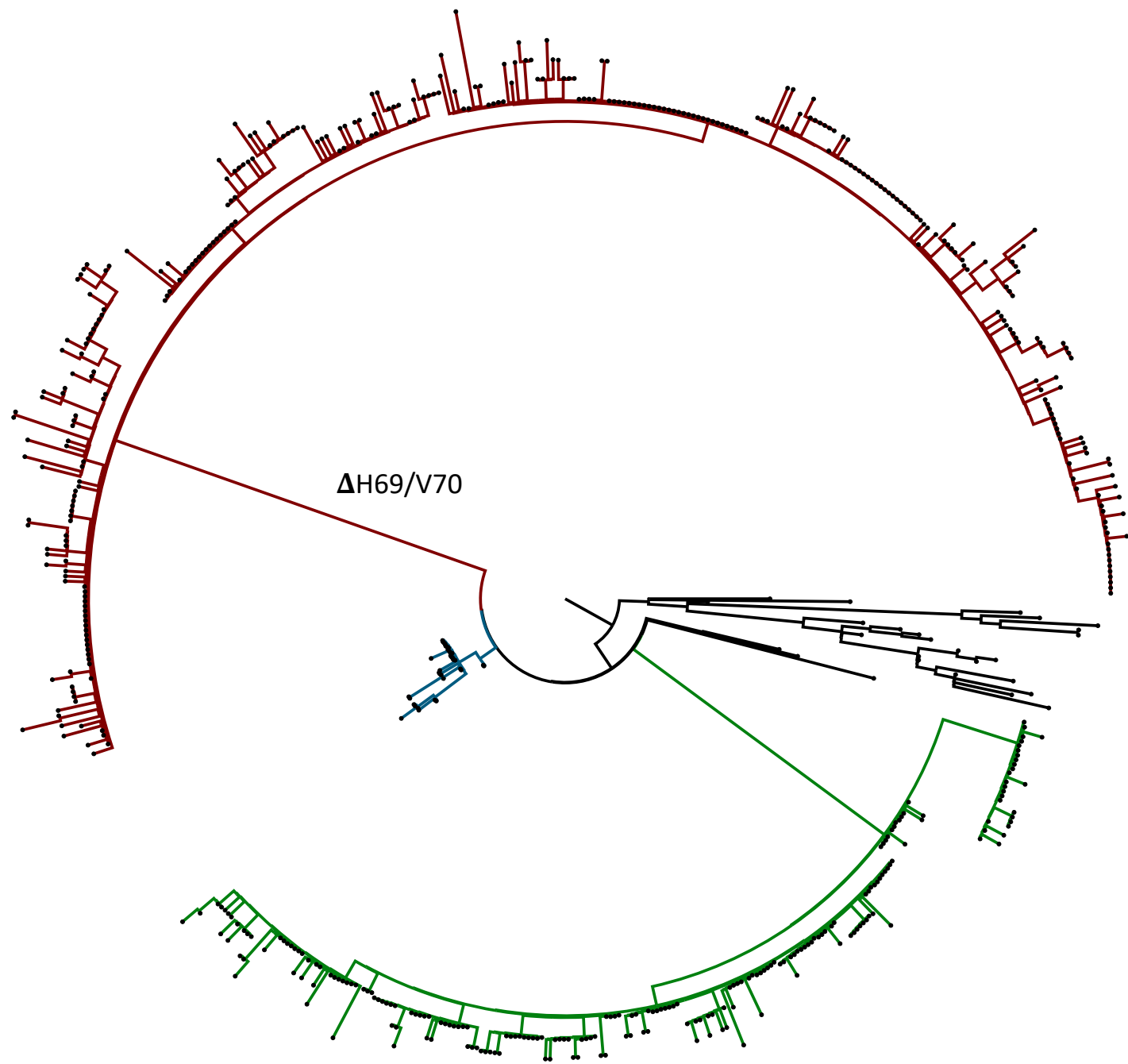


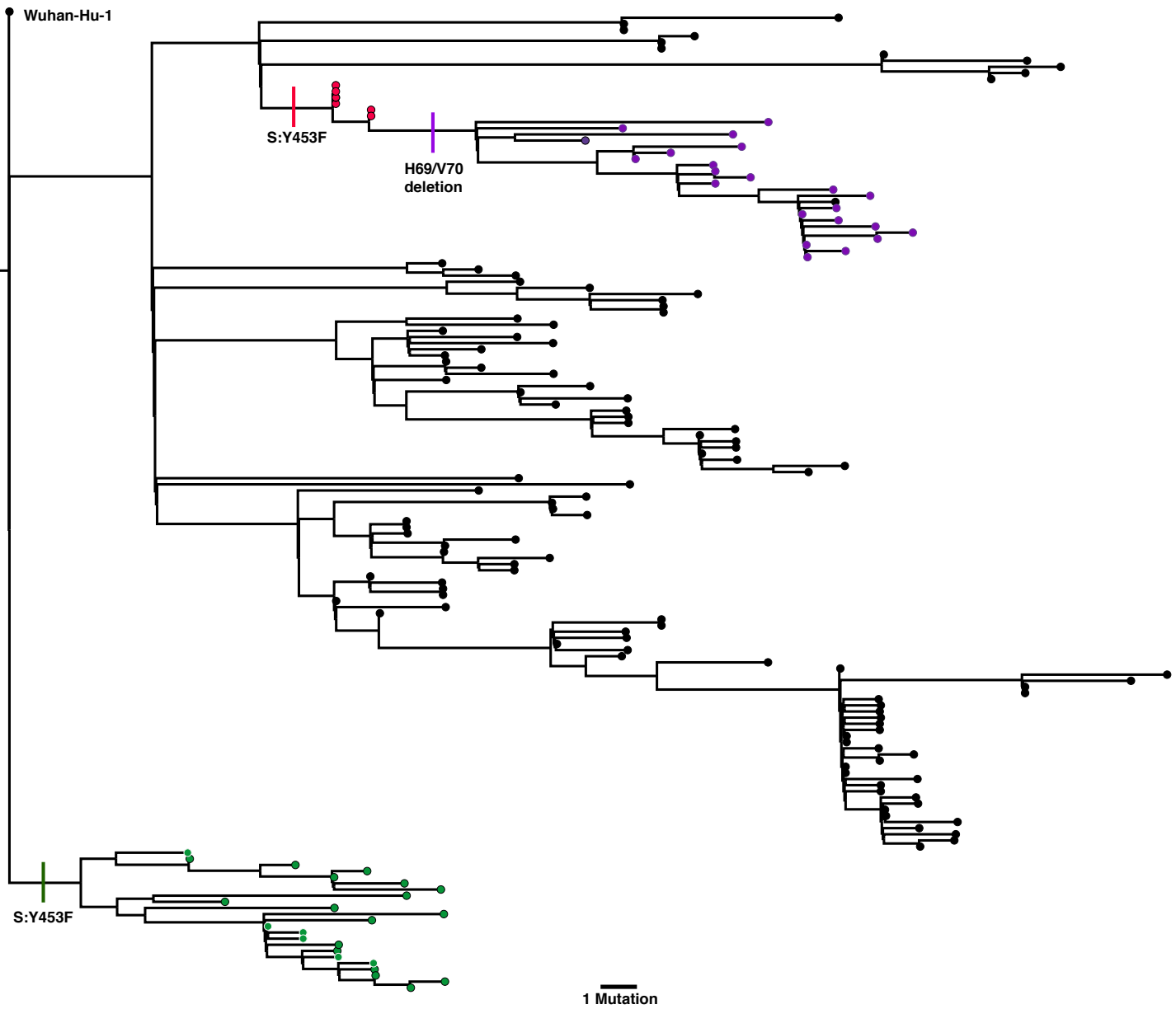
Figure 7: Spike mutant $\Delta H69/V70$ has 2 fold higher infectivity compared to wild type (D614G background) A and B. Single round Infection of target cells A and B by luciferase expressing lentivirus pseudotyped with SARS-CoV-2 Spike protein (WT versus mutant) on A. 293T cells co-transfected with ACE2 and TMPRSS2 plasmids and B. HeLa cells stably expressing ACE2. C. Data showing Infectivity normalized for virus input using reverse transcriptase activity in virus supernatants. RLU – relative light units; U – unit of reverse transcriptase activity. Data are representative of 2 independent experiments.



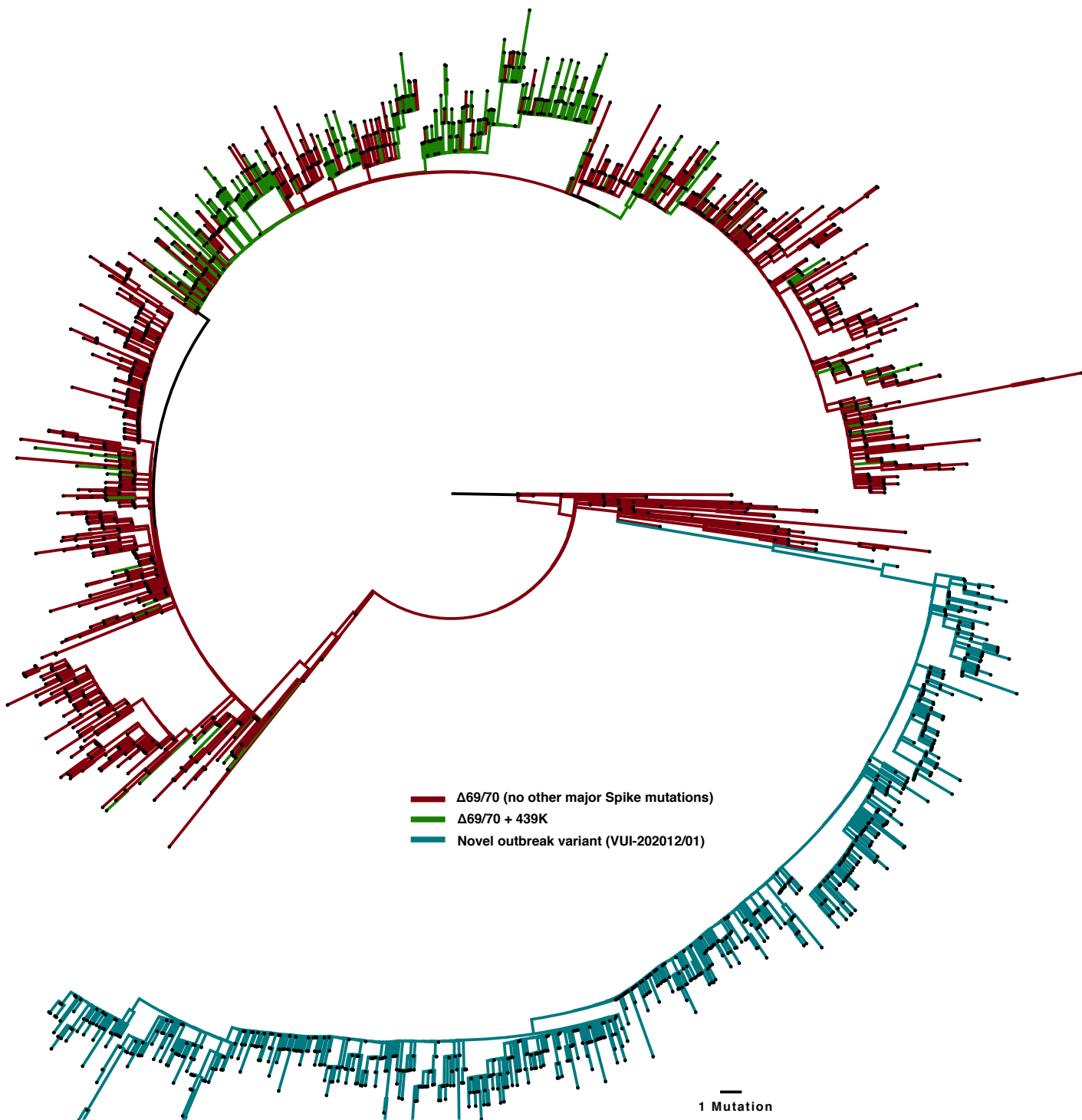
Supplementary Figure 1. Circularised maximum likelihood phylogeny of global sequences carrying Spike mutant 439K. All sequences in the GISAID database containing S:439K (3820 sequences, 26th November 2020) were realigned to Wuhan-Hu-1 using MAFFT. Viruses carrying the Spike double Δ tion Δ H69/V70 (red) emerged and expanded from viruses with S:439K (black).



Supplementary Figure 2. Circularised maximum likelihood phylogeny of global sequences carrying Spike mutant 501Y. All sequences in the GISAID database containing S:501Y were downloaded and realigned to Wuhan-Hu-1 using MAFFT. Sequences were broadly split into four major clades; sequences carrying the Spike double Δ etion $\Delta H69/V70$ (red) formed an entirely separate clade from non-carriers. Sequences carrying 501Y but an absence of $\Delta H69/V70$ formed a second lineage and appeared to expand only in Wales (green). Another major clade (blue) was limited entirely to Australia and finally a fourth clade (black) was limited to several African countries and Brazil.



Supplementary Figure 3. Maximum likelihood phylogenetic tree of mink-origin SARS-CoV-2 sequences. All 753 sequences in the GISAID database (accessed 14th December 2020) were downloaded and realigned to Wuhan-Hu-1 using MAFFT. Two distinct lineages carrying the mink-associated Spike Y453F mutations can be seen in Danish (red) sequences, with a separate lineage isolated only in Netherlands (green). After acquiring the Y453F mutation, Danish mink also appeared to acquire the Spike Δ etion Δ H69/V70 (purple).



Supplementary Figure 3. Global whole-genome phylogeny of SARS-CoV-2 sequences carrying the Spike $\Delta H69/V70$ Δ etion. All sequences carrying the double- Δ etion were downloaded from the GISAID database (5000 sequences, 16th Dec) and aligned to the Wuhan-Hu-1 reference strain using MAFFT. All duplicate sequences were removed to create a representative sub-sample. The inferred phylogeny clearly shows several distinct lineages carrying $\Delta H69/V70$ in the absence of other major Spike mutations (red) and alongside RDB mutation 439K (green). N501Y lineages cluster within the outbreak variant lineage. Y453F sequences are lost after de-duplication. The novel outbreak lineage currently circulating in England carries eight co-occurring Spike mutations (cyan) in the RBD (N501Y, A570D), S1 ($\Delta H69/V70$ and $\Delta 144/145$) and S2 (P681H, T716I, S982A and D1118H).